

www.acsami.org Research Article

# Probing the Mechanism of Targeted Delivery of Molecular Surfactants Loaded into Nanoparticles after Their Assembly at Oil—Water Interfaces

Mohamed Amen Hammami, Antonios Kouloumpis, Genggeng Qi, Ahmed Wasel Alsmaeil, Bashayer Aldakkan, Mazen Y. Kanj, and Emmanuel P. Giannelis\*



Cite This: https://doi.org/10.1021/acsami.2c18762



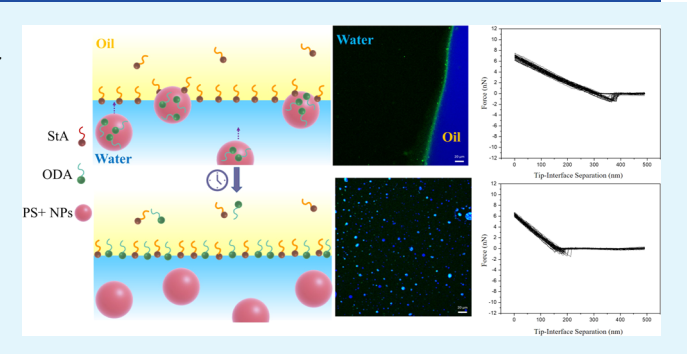
**ACCESS** I

III Metrics & More

Article Recommendations

Supporting Information

ABSTRACT: A targeted and controlled delivery of molecular surfactants at oil—water interfaces using the directed assembly of nanoparticles, NPs, is reported. The mechanism of NP assembly at the interface and the release of molecular surfactants is followed by laser scanning confocal microscopy and surface force spectroscopy. The assembly of positively charged polystyrene NPs at the oil—water interface was facilitated by the introduction of carboxylic acid groups in the oil phase (e.g., by adding 1 wt % stearic acid to hexadecane to produce a model oil). The presence of positively charged NPs consistently lowers the stiffness of the water—oil interface. The effect is lessened, when the NPs are present in a solution of NaCl or deionized water at pH 2, consistent with a less



dense monolayer of NPs at the interface in the last two systems. In addition, the NPs reduce the interfacial adhesion (i.e., the "stickiness" of the interface or, put differently, the pull-off force experienced by the atomic force microscopy (AFM) tip during retraction). After the assembly, the NPs can release a previously loaded cargo of surfactant molecules, which then facilitate the formation of a much finer oil—water emulsion. As a proof of concept, we demonstrate the release of octadecyl amine, ODA, that has been incorporated into the NPs prior to the assembly. The release of ODA causes the NPs to detach from the interface altering the interfacial properties and leads to finer oil droplets. This approach can be exploited in applications in several fields ranging from pharmaceutical and cosmetics to hydrocarbon recovery and oil-spill remediation, where a targeted and controlled release of surfactants is wanted.

KEYWORDS: nanoparticles, surfactants, oil-water interface, directed assembly, targeted delivery

#### ■ INTRODUCTION

Directed assembly of nanoparticles (NPs) at liquid-liquid interfaces has received widespread attention and has been extensively studied by numerous investigators. The use of the water-oil interface as a platform to direct, assemble, and manipulate NPs opens new opportunities for research in diverse fields, including colloidosomes, 1-3 stabilized Pickering emulsion,<sup>4-7</sup> drug delivery,<sup>8,9</sup> and all-liquid 3D printing.<sup>10-12</sup> An effective approach for the controlled assembly of NPs at the oil-water interface is by modulating and controlling the interactions (e.g., ion-pairing) between the NPs and the liquids. Examples of such systems consist of NPs dispersed in one of the liquid phases and a molecule with complementary functionality, which is added in a second, immiscible liquid phase. In this direction, the assembly of various nanomaterials, such as NPs, 13-16 graphene oxide nanosheets, 17,18 cellulose nanocrystals, <sup>19</sup> polyoxometalates, <sup>20</sup> and carbon nanotubes, <sup>21</sup> has been used to stabilize emulsions and to shape liquids into complex structures. Although various systems based on NPs acting as surfactants have been studied, reports of delivery of molecular surfactants in a targeted fashion after assembly of the NPs are still limited. Controlled delivery of surfactants at or near oil—water interfaces would alleviate some key challenges of using neat surfactants including extraneous adsorption or dilution (e.g., near wellbore at an injection site), which reduce their effectiveness. To reduce surfactant loss, several groups explored the use of nano-encapsulated systems as an alternative method for efficient surfactant delivery. For example, Avila et al. <sup>23</sup> evaluated the use of polystyrene NPs to encapsulate ionic (sodium dodecyl sulfate) and nonionic (nonyl-phenol ethoxylate-10) surfactants, which can be released by an oil

Received: October 18, 2022 Accepted: January 13, 2023



uptake-triggered swelling. Zhao and co-workers<sup>24</sup> explored a nanofluid system by immobilizing an anionic surfactant to amino-terminated silica NPs via electrostatic interactions. In addition, Nourafkan et al.<sup>25</sup> proposed porous TiO<sub>2</sub> as nanocarriers to deliver a blend of surfactants consisting of nonionic (alcohol ethoxylated) and anionic (alkyl aryl sulfonic acid) surfactants. They reported a reduced surface interaction of the surfactant molecules with the rock surface. Silica NPs have been also explored as nanocarriers for surfactant delivery. However, the easy dissociation of the surfactant molecules from the nanocarriers due to the relatively weak, non-covalent interactions limits to some extent the controlled release capabilities of these systems. Lastly, the addition of sacrificial chemicals has been explored to lower the surfactants loss, but these chemicals could increase implementation costs in real applications.<sup>26</sup> A potential solution is to deploy a system with targeted and controlled release capabilities analogous to those used in biomedicine to treat diseases. 27,28 Toward this end, we demonstrate here an NP system that first assembles at oilwater interfaces and subsequently releases a molecular surfactant (octadecyl amine, ODA) resulting in a finer emulsion.

Our system combines into one platform feature that allows first the assembly of NPs followed by the release of molecular surfactants. The assembly is facilitated by using positively charged NPs dispersed in the aqueous phase, which are electrostatically attracted to the negatively charged model-oil phase. We note that this approach is different from previous reports, where the NPs are used in place of surfactants (i.e., Pickering emulsions). Instead, the NPs are used as carriers of a water-insoluble molecular surfactant that is only released after the NPs assemble at the oil—water interface. Our work is also different from various other approaches 29-31 used for controlled release of surfactants as those involve a slow but not targeted release. Thus, even though the latter represent an improvement over the deployment of neat surfactants, they still suffer from some of the same efficacy issues mentioned above.

Our study shows that the NP assembly as followed by a number of techniques including confocal microscopy and force spectroscopy measurements can be modulated by employing different salinity electrolytes or by tuning the pH of the aqueous phase. Using the same probes, we were able for the first time to study the mechanism of the surfactant release and offer insights that can be used in practical applications. To the best of our knowledge, this is the first demonstration of both a targeted and controlled delivery of molecular surfactants at the interface to enhance emulsification.

## EXPERIMENTAL SECTION

**Materials and Methods.** Hexadecane, Nile red, cetyltrimethy-lammonium bromide (CTAB), 4,4-bis(2-benzoxazolyl) dye, stearic acid, sodium chloride (NaCl), calcium chloride dihydrate (CaCl $_2$ -2H $_2$ O), magnesium chloride hexahydrate (MgCl $_2$ -6H $_2$ O), sodium sulfate (Na $_2$ SO $_4$ ), sodium bicarbonate (NaHCO $_3$ ), and ODA (C $_{18}$ H $_{37}$ NH $_2$ ) were purchased from Sigma-Aldrich and used without further purification.

For the preparation of model oil, 0.01 M stearic acid was dissolved in hexadecane by stirring overnight at 50 °C. 4,4-bis(2-cetyltrimethylammonium) dye was used to add a fluorescent label that emits blue light for the LSCM (Laser Scanning Confocal Microscopy) imaging. For the preparation of seawater (SW) (hereafter, referred to as 100% SW), 41.04 g NaCl, 2.384 g CaCl<sub>2</sub>·2H<sub>2</sub>O, 17.645 g MgCl<sub>2</sub>·6H<sub>2</sub>O, 6.343 g Na<sub>2</sub>SO<sub>4</sub>, and 0.165 g NaHCO<sub>3</sub> were dissolved in 1 L

deionized (DI) water. This stock solution was further diluted with DI water to prepare solutions of 20 and 50% SW.

Polystyrene NPs were synthesized via free radical miniemulsion polymerization. Nile red was incorporated into the NPs to render them fluorescent and distinguishable from the oil phase. Positively or negatively charged NPs were synthesized using an ionic initiator and copolymerization of the corresponding ionic functional monomers. Briefly, for the positively charged PS NPs, 0.64 g of [2-(acryloyloxy)ethyl]trimethylammonium chloride, 0.75 g of CTAB, and 0.75 g of 2,2'-azobis(2-methylpropionamidine) dihydrochloride were dissolved in 300 g of DI water. The oil phase containing 60 g of styrene, 1 mg of Nile red, and 2 g of hexadecane was added to the aqueous solution and sonicated using a Branson Ultrasonics 450 Digital Sonifier for 15 min. The obtained milky emulsion was purged with N<sub>2</sub>, heated to 67 °C, and kept at that temperature for 12 h. The resulting PS NPs were purified via dialysis against DI water. Negatively charged polystyrene NPs were synthesized using the same procedure, except that 1.08 g of 3-allyloxy-2-hydroxy-1-propanesulfonic acid sodium salt solution, 0.58 g of sodium bicarbonate, and 0.85 g of sodium persulfate were used in the aqueous phase.

The ODA-loaded polystyrene NPs were synthesized similarly to the positively charged NPs described above, except that 3 g of ODA were added to the oil phase, and the fluorescent tag, Nile red, was replaced with the covalently bonded fluorescein to avoid leaching of the dye out of the NPs.

Apparatus and Methods. Transmission electron microscopy (TEM) images were obtained using an FEI Tecnai 12 BioTwin microscope. Confocal microscopy images were obtained using a Zeiss LSM 710 confocal laser scanning microscope with a Plan-Apochromat ×25 and 1.40 water-immersion objective. Emulsions were prepared by vortexing equal amounts of model oil with an aqueous suspension containing different amounts of the NPs (0.5-1 mg/mL) in DI water or brine. The pH of charged NPs dispersed DI water was adjusted to 2, 4, and 7 by adding aliquots of 0.1 M HCl and 0.1 M NaOH, as needed. A few milliliters of the mixture were placed between two coverslips and imaged. Zeta potential measurements were carried out using a Zetasizer Nano ZS90 (Malvern Instruments). Zeta potential was determined at 25 °C, and the NP suspensions (1 wt %) were sonicated for 30 min before each measurement using a water bath sonicator. For the emulsions, 2 mL of model oil was added to 5 mL of water and utilized in an ultrasonicator (Fisher Scientific, Q500) at 10% amplitude for 10 min. For time-dependent measurements, 4 mL of model oil was added to 8 mL of an aqueous dispersion containing the ODA-loaded NPs and mixed using an ultrasonicator. AFM experiments were performed in tapping and peak force tapping modes on a Multimode 8, Nanoscope 6, using sharp nitride lever (SNL-10) probes and Peakforce-HIRS-F-A cantilevers. For imaging in air, the positively charged PS NPs were deposited from aqueous dispersions onto silicon wafers (p-type Si, single side polished, purchased from Pure Wafer) by drop casting. For the oil-water interface measurements, a fluid cell was used, and the force-separation curves were obtained with a force of 7 nN, in all systems. The deflection sensitivity of the photodetector was calibrated by acquiring approach-retract curves on a sapphire sample in model oil; the spring constant of the cantilever was calibrated using the thermal method. A small droplet of the aqueous solution with or without the NPs was placed on the silicon wafer, and a larger drop of model oil was added to completely cover the water droplet. For reproducible results, the AFM tip and tip holder were immersed first in a few drops of model oil prior to the measurements. The interfacial tension (IFT) of oil in aqueous suspension of NPs was determined using a spinning-drop tensiometer (KRUSS). The suspension was withdrawn into a 3.25 mm in diameter capillary tube and an oil droplet of 4 µL was released into the suspension. The equilibrium IFT was determined when three consecutive measurements did not fluctuate more than 10%.

# ■ RESULTS AND DISCUSSION

**Directed Assembly of the NPs at the Oil-Water Interface.** We started by investigating the mechanism of NP

assembly using the model oil-water mixture. Recall that the model oil is prepared by adding 1 wt % of stearic acid into hexadecane. The fluorescent, water-dispersible polystyrene NPs were synthesized via free-radical emulsion polymerization, as described in the experimental section and shown in Scheme S1. A quaternary ammonium comonomer was used to produce positively charged polystyrene NPs (PS+). We note that the negatively charged polystyrene NPs used for control experiments were synthesized by the same method and substituting the quaternary ammonium with a sulfonate comonomer. Both positive and negative NPs are dispersible in DI water and various brines. TEM and AFM imaging analyses showed uniform, non-aggregated spherical particles with an average diameter of 173 and 151 nm for PS+ and PS-, respectively (Figure S1, of the supporting information). The zeta potential of the NPs in DI water was +41 and -43 mV for the PS+ and PS- NPs, respectively (Figure 1). Since the carboxylate groups of stearic acid segregate at the surface, the z-potential of model oil at pH 7 is -34 mV.

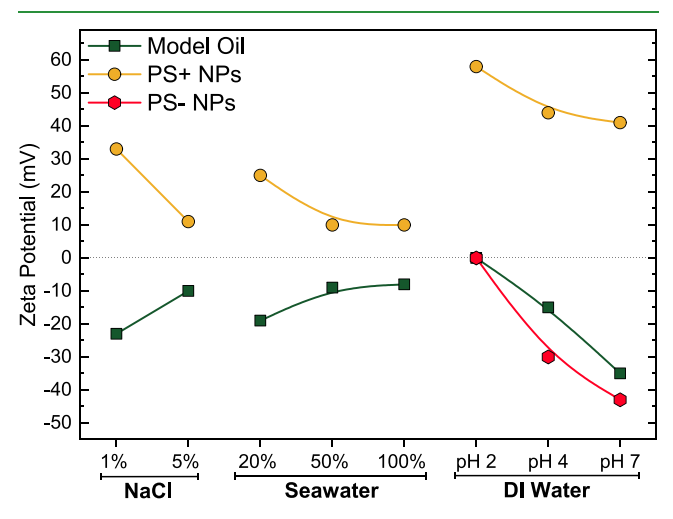


**Figure 1.** Zeta-potential measurements of model oil, PS+, and PS-NPs at different brines and pHs.

When a mixture of equal volumes of water and model oil is vigorously agitated in a vortex mixer, it forms a non-uniform emulsion, which phase-separates quickly into the two immiscible phases. In contrast, when positively charged NPs are added in the aqueous phase a different behavior and a more stable emulsion are observed. LSCM images, in Figure 2A,B, show clearly that the positively charged NPs tend to segregate at the oil—water interface attracted by the negatively charged carboxylate groups in the oil phase. Moreover, imaging of the oil droplet at different depths demonstrates that the red fluorescent NPs decorate the surface of the model oil droplet (blue light fluorescence) uniformly, as shown in Figure 3.

AFM was used to provide direct visualization of the NP assembly at the water—oil interface. Following established protocols developed for liquid—liquid interfacial imaging, <sup>32–35</sup> the AFM tip (immersed through the oil phase) is brought into contact with the aqueous phase. The AFM image in Figure 2D shows a near closed-packed assembly of NPs decorating the interface. The amount of coverage of the interface is dependent on the concentration of NPs in the aqueous phase (lower concentrations lead to reduced coverage). The NPs after assembly are virtually immobile, except when a low concentration of NPs is used leading to a low coverage,

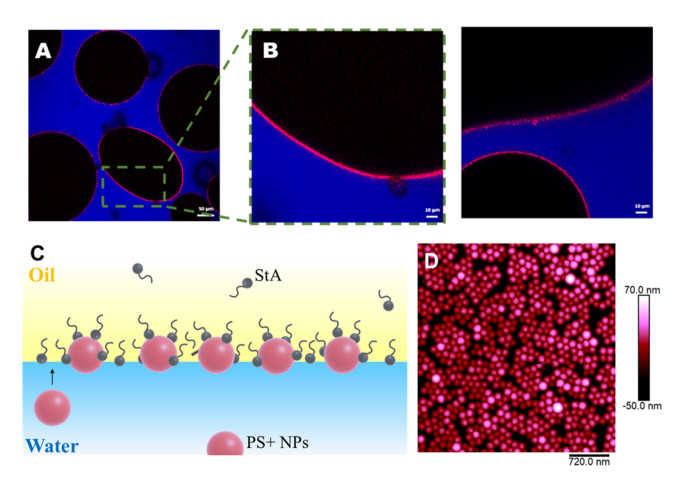


**Figure 2.** (A, B) LSCM images for an equal volume mixture of model oil and DI water, showing the attachment and assembly of PS+ NPs in the DI water-model oil interface. In all images, the NPs are labeled with a red fluorescent dye and the oil phase with a blue fluorescent dye. (C) Schematic representation and (D) AFM height image of PS+ NPs assembly at the DI water-model oil interface.

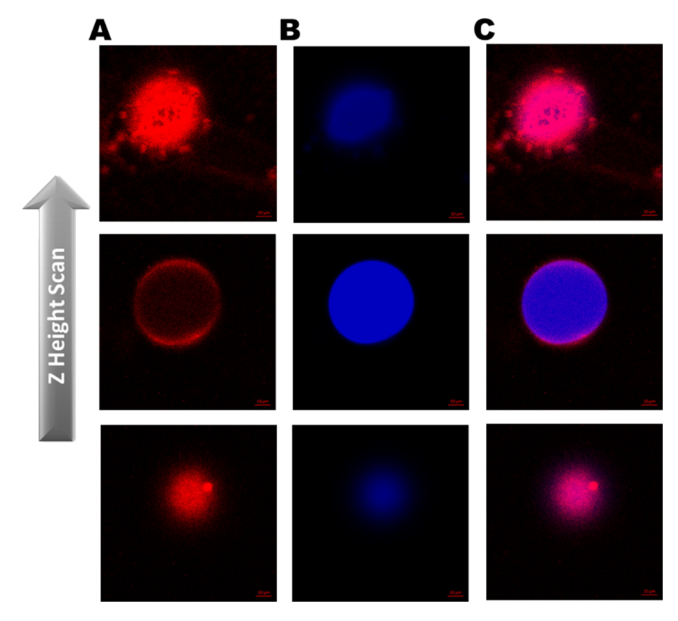


**Figure 3.** Three-dimensional confocal images (z-scans) taken at various depths showing the uniform assembly of the PS+ NPs around an oil droplet with increasing depth (bottom, middle, and top of an oil droplet). (A) Red filter showing the NPs only, (B) blue filter showing the oil only, and (C) overlap of the two.

where the NPs show a very small degree of mobility at the early stages of assembly (Figure S3). Interestingly, the size of the assembled NPs at the interface measured by in situ AFM (110 nm) is smaller than that measured by TEM after drying a water suspension (173 nm) suggesting that the NPs do not partition equally at the interface but prefer to be more in the oil phase.

The above are consistent with dynamic IFT measurements, showing that the assembly of positive NPs at the oil—water interface reduces the IFT of the mixture from 31 to 11 mN/m. These results are contrasted with experiments performed with the negatively charged, sulfonate-functionalized NPs under the same conditions (Figure S2A). In the absence of an electrostatic driving force, the negatively charged NPs are

not directed to the oil-water interface and stay dispersed in the aqueous phase. These experiments demonstrate that the complementarity of charges at the interface is required to provide the necessary interactions for a successful assem- $\bar{b}$ ly.  $^{35-3}$ 

To evaluate the effect of salinity on the directed assembly, a series of suspensions of positive NPs in brines of varying composition and ionic strength were used in place of DI water (Figure 4). The results of suspensions of positively charged

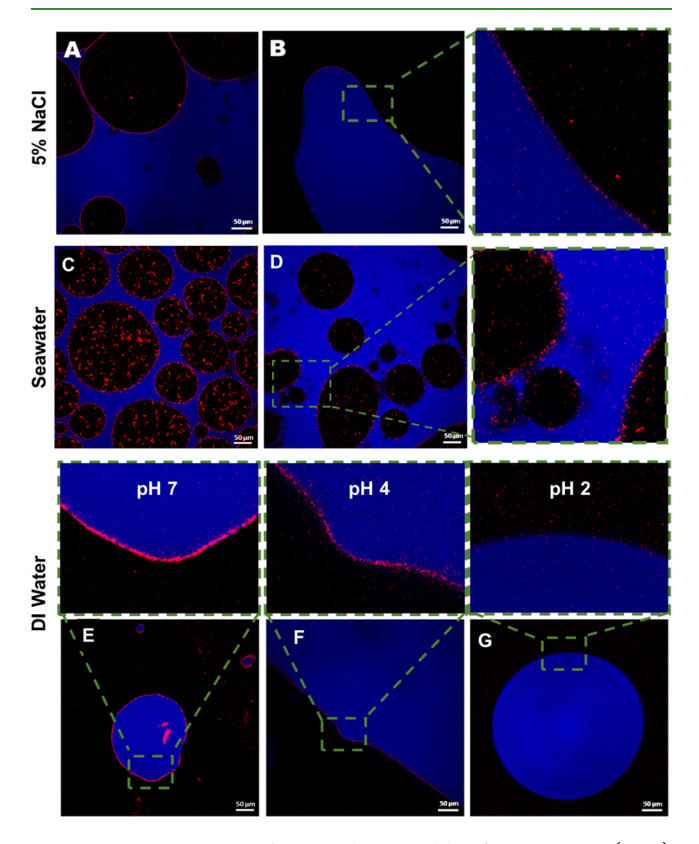


Figure 4. LSCM images showing the assembly of PS+ NPs, in (A, B) 5% NaCl, (C, D) 100% seawater, as well as in (E) pH 7, (F) 4, and (G) 2.

NPs in water containing 1 and 5 wt % of NaCl after mixing with oil are shown in Figures S4 and 4A,B, respectively. Consistent with NaCl screening the surface charges, the zeta potential of both oil and NPs decreases with increasing salt concentration (Figure 1). Nevertheless, and despite the weakened ionic interactions, the positively charged NPs are attracted and assembled at the interface. The degree of segregation and assembly at the interface becomes less with increasing NaCl concentration, consistent with the reduced charge on both the NPs and the oil.

In addition, we tested three different NP suspensions in a mixture of electrolytes simulating SW as well as lower salinity brines obtained by diluting SW in DI water to produce solutions of 20 and 50% (Figure S5). Increasing ionic strength results in a decrease of the charge in both NPs and oil, but both NPs and oil remain oppositely charged (10 and -9 mV, respectively) even when the highest salinity brine is used (Figure 2C,D). As expected, the NPs remain attracted to and segregate at the interface, although the coverage is less than in DI water. The reduced coverage is consistent with the lowering (in absolute value) of the charge on both the NP and oil.

Another factor that affects the electrostatic interactions is pH. At pH 7, the carboxylic groups are deprotonated, and the surface charge of the oil is negative, while the ammonium decorated NPs are protonated and positive (Figure 1). The same is true for pH 4, although the charge is lower in both systems. This charge complementarity gives rise to strong electrostatic interactions and leads to a uniform decoration of the NPs at the interface (Figure 4E,F), with the higher charges on opposite surfaces leading to a stronger effect (pH 7 vs pH 4). However, under strong acidic conditions (pH  $\sim$  2), the oil becomes neutral and the positively charged NPs are no longer attracted to the interface despite the high charge (58 mV) on the NPs (Figure 4G). Interestingly, under these conditions, the PS- NPs still assemble at the interface (Figure S2B-D). The assembly, in this case, is facilitated by H-bonding between the sulfonic acid groups on the NPs and the carboxylic groups on the oil surface, most likely mediated by water molecules.

Nanomechanical Properties of Oil-Water Interfaces. To further study the assembly of the NPs and to develop a better understanding of the interactions involved, surface force spectroscopy was used. We note that force spectroscopy goes beyond mere imaging and provides information on the mechanical response of the interface. Figure S6 shows typical force-separation (F-S) curves for various systems when the same force (7 nN) is applied. In general, the slope of the curve in the contact region decreases in the presence of NPs, indicating a softer interface (softer interfaces lead to less cantilever deflection at the same height, z). From these measurements, the interfacial behavior is quantified (Figure S6C) and a detailed mechanical response can emerge, summarized in Figure 5. As we mentioned earlier, the assembly of positively charged NPs at the oil-water interface lowers the IFT of the mixture. Similarly, the interfacial stiffness, (Figure 5A), 32,33 consistently decreases with the presence of NPs in the oil-water interface, with the most notable differences observed, when the NPs are in DI water (decrease of 30 mN m<sup>-1</sup>) or SW (decrease of 35 mN m<sup>-1</sup>). The results for the system either in a solution of 5 wt % NaCl or at pH 2 show relatively minor changes (~7.5 mN m<sup>-1</sup>), when NPs are present in the aqueous phase, consistent with the presence of a submonolayer of NPs at the interface in these systems. The trend for the deformation is consistent with that for the modulus. For example, a more deformable interface is seen, when the oil is mixed with a suspension of NPs in either DI water (185 nm) or SW (145 nm) (Figure 5B), while the effect is minimal for NPs suspended in water containing 5 wt % NaCl (20 nm) or in water at pH 2 (10 nm).

In addition to stiffness and deformation, the force spectroscopy measurements provide information about adhesion. The "stickiness" of the interface is taken from the minimum of the force vs separation curves upon retraction of the (hydrophilic) tip. The mean adhesion of the interface between the oil and the NP-free water is 5 nN (Figure 5C). When the DI water is substituted with a brine containing NaCl (5 wt %) or with SW, the mean value of the adhesion remains virtually unchanged, although the values show a higher distribution. In contrast, when the pH of the aqueous phase is lowered to 2, the adhesion doubles, probably due to the decrease of the charge of the model oil to practically zero, making it essentially a neutral surface. When NPs are introduced into the aqueous phase, the adhesion or the "stickiness" of all systems is lower compared to the systems in the absence of NPs. These experiments suggest that the pull-off force experienced by the

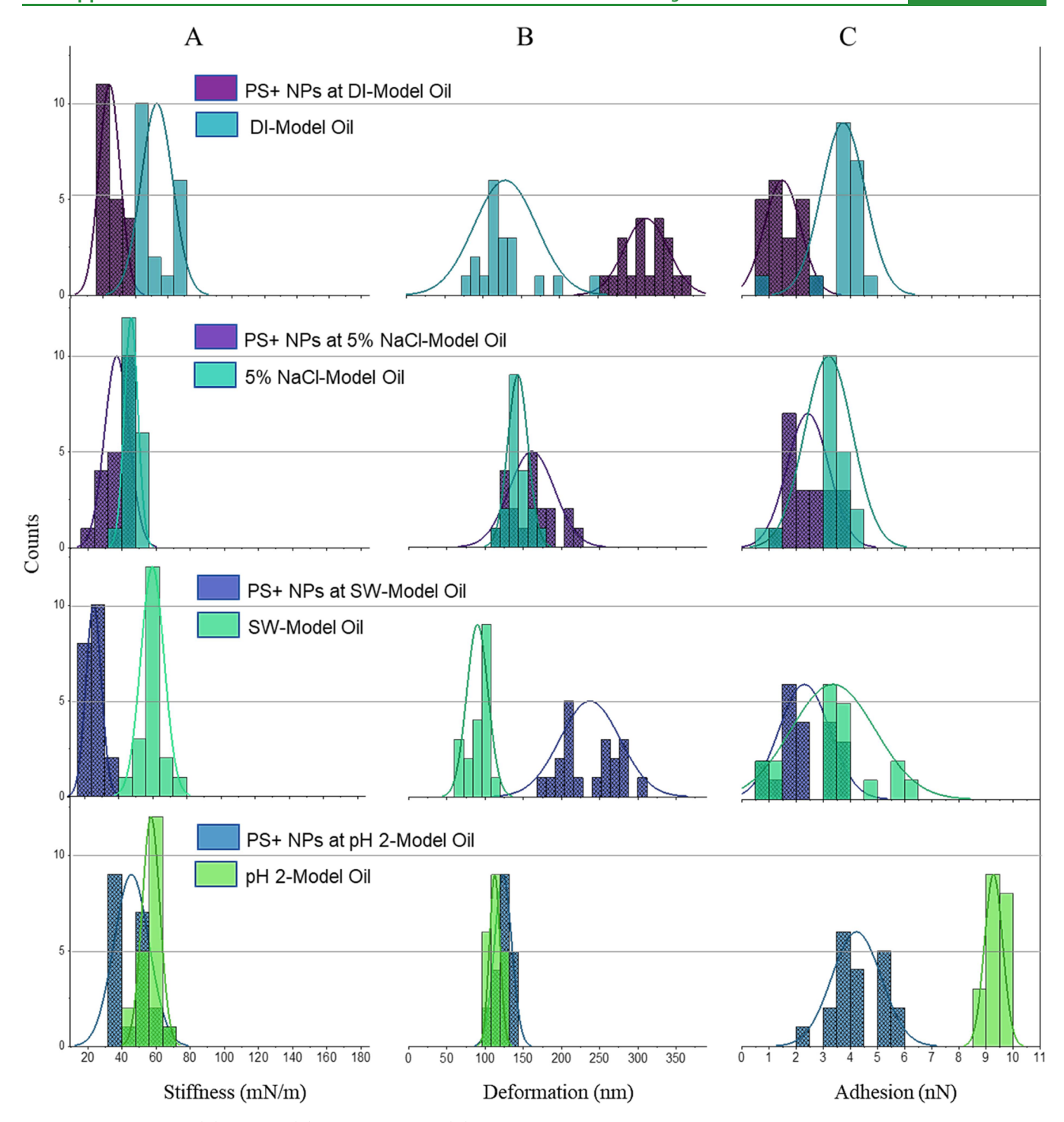


Figure 5. Histograms of (A) stiffness, (B) deformation, and (C) adhesion of various oil—water systems, in the presence and absence of NPs in the aqueous phase, derived from force—separation curves.

AFM tip during retraction, or the stickiness of the interface is reduced in the presence of the hydrophilic NPs. 40,41 At pH 2 an increased adhesion force is seen. We note that the model oil is basically neutral and the increased adhesion in the oil—water mixture in the absence of the NPs is attributed to the protonation of the carboxylic groups and the resulting charge neutralization that allows the stearic acid to form strongly interacting, H-bonded aggregates of stearic acid and neighboring water molecules. 42,43 In that case, a higher force is observed for the retraction of the AFM tip from the interface resulting from the increased adhesion. Interestingly, the presence of the

NPs in DI water at pH 2 decreases the adhesion to a value comparable to that of the neat oil—water system at neutral pH. The decrease is most likely due to the presence of the NPs at the interface where, even though the coverage is very sparse, the NPs disrupt the formation of strongly bonded, stearic acid aggregates leading to a lower adhesion. <sup>40,44</sup>

Mechanism of Targeted Delivery and Release. After studying systematically the electrostatic interactions and assembly in various systems, we investigated the potential of the assembled NPs to emulsify an oil—water mixture by releasing locally their surfactant loaded cargo. More specifi-

**ACS Applied Materials & Interfaces** 

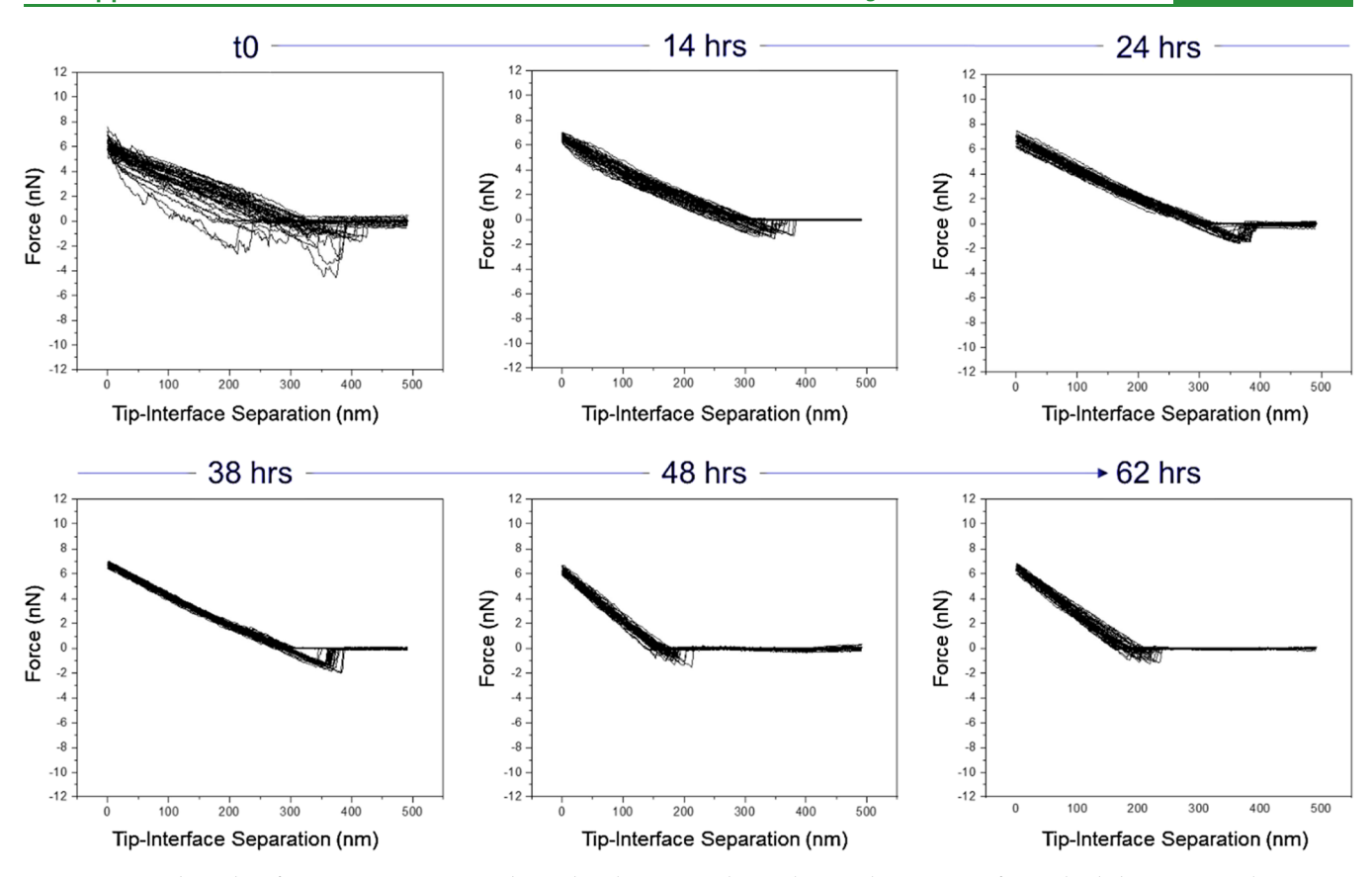


Figure 6. Time-dependent force—separation curves obtained in the water—oil interphase in the presence of ODA-loaded PS+ NPs in the aqueous phase.

cally, we investigated the release and delivery of a waterinsoluble molecular surfactant, ODA, which had been encapsulated during synthesis inside the NPs (Scheme S1). Note that for these studies the fluorescent tag, Nile red, was replaced with the covalently bonded fluorescein to avoid complications related to the leaching of Nile red out of the NPs and affecting emulsification. The assembly of the ODAloaded NPs as well as the surfactant release was studied by a series of time-resolved force spectroscopy measurements. Figure 6 shows force-separation curves for the water-oil interface in the presence of ODA containing NPs in the aqueous phase as a function of time. At t0 (taken 30 min after the model oil was added to an aqueous dispersion of NPs), the response is noisy exhibiting a range of stiffnesses and deformation values. The inhomogeneity of the interface, with both soft (NP decorated interface) and stiff (neat interface) regions, suggests that the assembly of the NPs is not instantaneous and that it takes time for the system to reach equilibrium. After 14 h, the force separation curves stabilize into a more uniform response and the mechanical properties are consistent with a system where NPs are present at the interface, as discussed above. This behavior persists for 38 h. Interestingly after 48 h, the mechanical properties change again, and the results correspond to a stiffer interface. No further changes are observed after 62 h.

Specifically at t0, the stiffness (Figure 7A) of the oil—water interface ranges from 18 to 49 mN/m; the lower values are similar to an oil—water mixture in the presence of NPs, while the higher values correspond to NP-free interfaces as discussed previously (Figure 5). The stiffness stabilizes at  $\sim$ 22 mN/m at t=38 h, and it becomes  $\sim$ 40 mN/m at t=48 h. Note that the

latter value is comparable to an NP-free system. The deformation of the interface follows an opposite trend (i.e., higher stiffness corresponds to lower deformation) (Figure 7B).

Based on the above, we propose the following mechanism of NP assembly and surfactant release. When the suspension of the NPs is mixed with the oil, there is a time lapse before the NPs assemble uniformly at the interface. The parts of the interface that are decorated with NPs show low stiffness (high deformation), while those that remain free of NPs show higher stiffness (low deformation) similar to the NP-free interfaces. As time passes, the NPs continue to assemble and after they reach a steady state, the behavior is similar to the NPdecorated interface. However, the release of the ODA (triggered by its solubilization in oil) forces the NPs to detach from the interface, and the mechanical behavior reverts to an oil-water interface that is no longer decorated by NPs. This detachment can be attributed to the presence of the ODA at the interface that weakens the electrostatic interactions between the oil and the NPs (see below). 45-48

The release of the ODA from the NPs, and the emulsification of the oil was confirmed macroscopically by confocal microscopy by comparing the images of an oil (20 wt %)—water mixture with and without NPs present in the aqueous phase. Figure 8B,C shows images of the mixture at t0 and t = 48 h, respectively. Figure 8A shows the mixture in the absence of the NPs. In the absence of NPs, a large-scale phase separation is seen (Figure 8A). When the NPs are present in the aqueous phase, the NPs assemble at the interface (t0, Figure 8B). Since no release of ODA has taken place yet, a large phase separation of the mixture is still apparent. However,

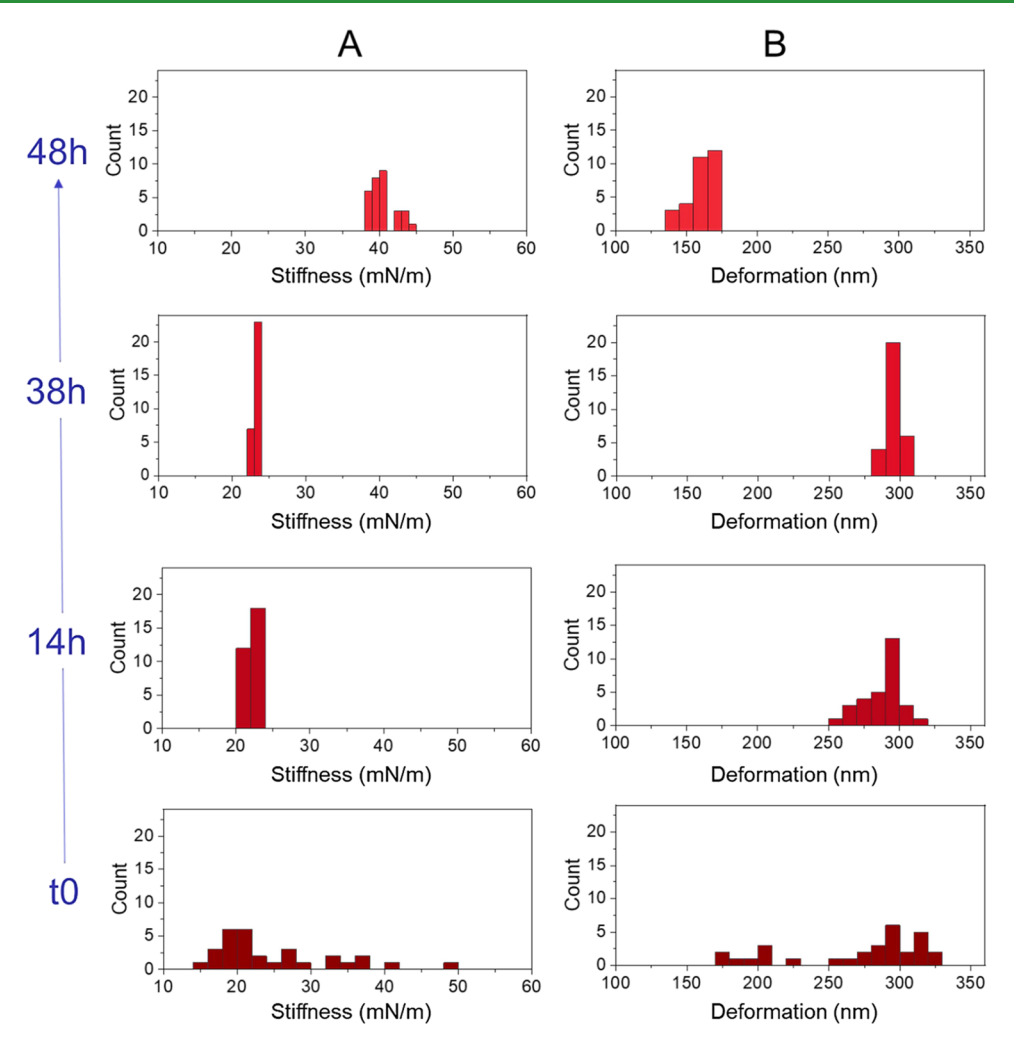


Figure 7. Histograms of (A) stiffness and (B) deformation, derived from force—separation curves of the water—oil system in the presence of ODA-loaded PS+ NPs in the aqueous phase.

an image taken after 48 h shows a finer oil—water emulsion with much smaller oil droplets ( $\sim$ 3  $\mu$ m in size) formed (Figure 8C).

The z-potential of the various systems involved was followed for further insights into the process. The ODA-loaded NPs show a z-potential of +32 mV (still positive but slightly lower than that of the ODA-free (Nile red based NPs described earlier); the model oil starts at -35 mV (Figure 8D).<sup>49-51</sup> When the oil and the aqueous suspension are mixed together and after about half an hour (t0), the majority of the emulsion shows a z-potential of -5 mV with a minority second peak at +32 mV. The results are consistent with oil droplets decorated with NPs with some free NPs remaining (-5 and +32 mV, respectively). After 14 h and with more NPs attracted to the interface the charge of the emulsion turns slightly positive. A smaller fraction shows a peak at -8 mV most likely due to oil that is not completely decorated with NPs. The emulsion reaches a maximum value of +10 mV after 24 h, decreasing to almost a neutral value after 48 h. Notably, on their own the NP suspensions as well as the model oil are fairly stable over time with virtually no changes in their z-potential. From the above and using the z-potential of oil-water mixtures intentionally spiked with ODA as a reference (Figure S7, left), we estimate the ODA release of the NPs to be about 20% of the total.

Based on the above, we suggest that early in the process the positively charged NPs are attracted by charge complementarity and assemble at the oil-water interface driven by the electrostatic interactions. After an equilibration time of a few hours, they start releasing their cargo. As ODA is released into the oil phase, it prevents the gross phase separation and forms a finer emulsion. In addition, as ODA is released, it displaces the NPs from the interface, which returns to the aqueous phase. It is worth mentioning that force spectroscopy of an intentionally ODA-spiked oil shows the same mechanical response as that measured after the slow release of ODA from the NPs (Figure S7, right). It is also worth mentioning that the intentionally spiked ODA oil shows an adhesion value similar to that at pH 2 in the absence of NPs where the oil phase is neutral and void of NPs. 52 Moreover, the IFT of the system, when the ODA-loaded NPs are present takes several hours to equilibrate and after 54 h, it plateaus at 2.7 mN/m. For comparison, the IFT of the system in the presence of NPs, which do not contain ODA, reaches quickly a value of 11 mN/ m.

#### CONCLUSIONS

In summary, the mechanism for targeted assembly of NPs and delivery of a water-insoluble molecular surfactant incorporated into their cores has been investigated by a number of

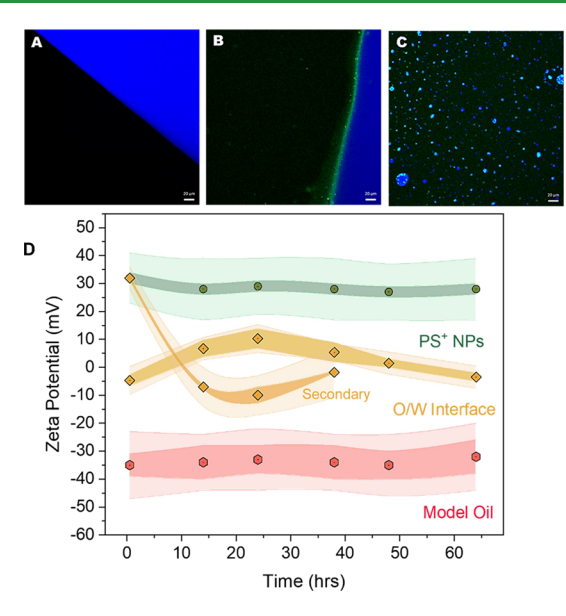


Figure 8. Top: LSCM images demonstrating the delivery of ODA to an oil—water mixture. (A) Water—model oil mixture; (B) aqueous dispersion of ODA-loaded PS+ NPs—oil mixture, right after mixing; (C) the same dispersion after 48 h. Bottom: Time-dependent zeta potential measurements (D) of the ODA-loaded NPs—model oil system, demonstrating the charges of water and model oil phases as well as of the emulsion. Data are represented as mean of  $\pm$  error bar and standard deviation (highest opacity), based on triplicate independent measurements.

techniques including for the first time force spectroscopy measurements. Positively charged NPs assemble preferentially at the oil-water interface by fine-tuning the electrostatic interactions with the negatively charged carboxylic groups present in the oil phase. The electrostatic interactions can be modulated by changing the ionic strength of the aqueous phase or the pH. The NPs influence the interfacial properties of the oil-water interface. For example, the stiffness of the interface decreases, and the deformability increases in the presence of the NPs. In addition, the NPs reduce interfacial adhesion. After the assembly, the NPs release an appropriately loaded cargo of surfactants, which facilitate the formation of a much finer oilwater emulsion. We further show that the release of ODA, which has been preloaded onto the NPs, causes the NPs to detach from the interface and leads to a finer emulsion with a smaller oil droplet size. These studies provide proof of concept for a targeted and controlled release and provide mechanistic insights of the process paving the way for a number of potential applications in diverse fields, where emulsions are used.

## ASSOCIATED CONTENT

# **Supporting Information**

The Supporting Information is available free of charge at https://pubs.acs.org/doi/10.1021/acsami.2c18762.

Synthetic procedure, TEM and AFM of NPs, confocal images of NPs in various brines, in situ AFM and force—separation curves obtained for PS+ NPs in various liquid—liquid interphases (PDF)

#### AUTHOR INFORMATION

## **Corresponding Author**

Emmanuel P. Giannelis – Department of Materials Science and Engineering, College of Engineering, Cornell University,

Ithaca, New York 14853, United States; Email: epg2@cornell.edu

#### Authors

Mohamed Amen Hammami – Department of Materials Science and Engineering, College of Engineering, Cornell University, Ithaca, New York 14853, United States; orcid.org/0000-0002-6162-3629

Antonios Kouloumpis — Department of Materials Science and Engineering, College of Engineering, Cornell University, Ithaca, New York 14853, United States; orcid.org/0000-0002-8738-3141

Genggeng Qi — Department of Materials Science and Engineering, College of Engineering, Cornell University, Ithaca, New York 14853, United States

Ahmed Wasel Alsmaeil — Department of the Chemical and Biomolecular Engineering, Cornell University, Ithaca, New York 14850, United States; orcid.org/0000-0001-7121-9876

Bashayer Aldakkan — Department of Materials Science and Engineering, College of Engineering, Cornell University, Ithaca, New York 14853, United States; orcid.org/0000-0001-9025-540X

Mazen Y. Kanj — Center for Integrative Petroleum Research (CIPR), College of Petroleum Engineering and Geosciences, King Fahd University of Petroleum and Minerals, Dhahran, KSA 31261, Saudi Arabia; orcid.org/0000-0002-2674-4505

Complete contact information is available at: https://pubs.acs.org/10.1021/acsami.2c18762

# **Author Contributions**

E.P.G. and M.Y.K. conceived and guided the project; G.Q. and B.A. synthesized the samples; A.K. and M.A.H. characterized the samples and the liquid—liquid interfaces; A.W.A. performed the IFT measurements. The manuscript was written with contributions of all authors. M.A.H. and A.K. contributed equally.

#### Notes

The authors declare no competing financial interest.

# ACKNOWLEDGMENTS

This publication is based on work supported by the College of Petroleum Engineering and Geosciences, King Fahd University of Petroleum and Minerals. The authors acknowledge Dr. Senli Guo (Bruker Inc.) for his assistance with the initial AFM experiments. This work made use of the Cornell Center for Materials Research Shared Facilities, which are supported through the NSF MRSEC program (DMR-1719875). Imaging data were acquired through the Cornell Institute of Biotechnology's Imaging Facility, with NIH 1S10OD010605 funding for the shared Andor Revolution Spinning Disk Confocal Microscope.

# **■** REFERENCES

- (1) McGorty, R.; Fung, J.; Kaz, D.; Manoharan, V. N. Colloidal Self-Assembly at an Interface. *Mater. Today* **2010**, *13*, 34–42.
- (2) Dou, H.; Li, M.; Qiao, Y.; Harniman, R.; Li, X.; Boott, C. E.; Mann, S.; Manners, I. Higher-Order Assembly of Crystalline Cylindrical Micelles into Membrane-Extendable Colloidosomes. *Nat. Commun.* **2017**, *8*, 426.
- (3) Dinsmore, A. D.; Hsu, M. F.; Nikolaides, M. G.; Marquez, M.; Bausch, A. R.; Weitz, D. A. Colloidosomes: Selectively Permeable

- Capsules Composed of Colloidal Particles. Science 2002, 298, 1006–1009.
- (4) Amalvy, J. I.; Armes, S. P.; Binks, B. P.; Rodrigues, J. A.; Unali, G. F. Use of Sterically-Stabilised Polystyrene Latex Particles as a PH-Responsive Particulate Emulsifier to Prepare Surfactant-Free Oil-in-Water Emulsions. *Chem. Commun.* **2003**, *3*, 1826–1827.
- (5) Zhou, J.; Wang, L.; Qiao, X.; Binks, B. P.; Sun, K. Pickering Emulsions Stabilized by Surface-Modified Fe3O4 Nanoparticles. *J. Colloid Interface Sci.* **2012**, 367, 213–224.
- (6) Sakthivel, S.; Zhou, X.; Giannelis, E. P.; Kanj, M. Y. Carbon Nanodots for Enhanced Oil Recovery in Carbonate Reservoirs. *Energy Rep.* **2021**, *7*, 8943–8959.
- (7) Al-Shatty, W.; Campana, M.; Alexander, S.; Barron, A. R. Interaction of Surface-Modified Alumina Nanoparticles and Surfactants at an Oil/Water Interface: A Neutron Reflectometry, Scattering, and Enhanced Oil Recovery Study. ACS Appl. Mater. Interfaces 2022, 14, 19505–19514.
- (8) Frelichowska, J.; Bolzinger, M. A.; Valour, J. P.; Mouaziz, H.; Pelletier, J.; Chevalier, Y. Pickering w/o Emulsions: Drug Release and Topical Delivery. *Int. J. Pharm.* **2009**, *368*, 7–15.
- (9) Xia, Y.; Wei, J.; Du, Y.; Wan, T.; Ma, X.; An, W.; Guo, A.; Miao, C.; Yue, H.; Li, S.; Cao, X.; Su, Z.; Ma, G. Exploiting the Pliability and Lateral Mobility of Pickering Emulsion for Enhanced Vaccination. *Nat. Mater.* **2018**, *17*, 187–194.
- (10) Forth, J.; Liu, X.; Hasnain, J.; Toor, A.; Miszta, K.; Shi, S.; Geissler, P. L.; Emrick, T.; Helms, B. A.; Russell, T. P. Reconfigurable Printed Liquids. *Adv. Mater.n* **2018**, *30*, No. 1707603.
- (11) Feng, W.; Chai, Y.; Forth, J.; Ashby, P. D.; Russell, T. P.; Helms, B. A. Harnessing Liquid-in-Liquid Printing and Micropatterned Substrates to Fabricate 3-Dimensional All-Liquid Fluidic Devices. *Nat. Commun.* **2019**, *10*, 1095.
- (12) Xu, R.; Liu, T.; Sun, H.; Wang, B.; Shi, S.; Russell, T. P. Interfacial Assembly and Jamming of Polyelectrolyte Surfactants: A Simple Route to Print Liquids in Low-Viscosity Solution. *ACS Appl. Mater. Interfaces* **2020**, *12*, 18116–18122.
- (13) Keane, R. K.; Hong, W.; He, W.; Teale, S.; Bancroft, R.; Dinsmore, A. D. Adsorption of Hydrophilic Silica Nanoparticles at Oil-Water Interfaces with Reversible Emulsion Stabilization by Ion Partitioning. *Langmuir* **2022**, *38*, 2821–2831.
- (14) Wang, M.; Zhang, Z.; He, J. A SERS Study on the Assembly Behavior of Gold Nanoparticles at the Oil/Water Interface. *Langmuir* **2015**, *31*, 12911–12919.
- (15) Lee, J. G.; Larive, L. L.; Valsaraj, K. T.; Bharti, B. Binding of Lignin Nanoparticles at Oil-Water Interfaces: An Ecofriendly Alternative to Oil Spill Recovery. ACS Appl. Mater. Interfaces 2018, 10, 43282–43289.
- (16) Li, R.; Chai, Y.; Jiang, Y.; Ashby, P. D.; Toor, A.; Russell, T. P. Carboxylated Fullerene at the Oil/Water Interface. *ACS Appl. Mater. Interfaces* **2017**, *9*, 34389–34395.
- (17) Fang, S.; Chen, T.; Wang, R.; Xiong, Y.; Chen, B.; Duan, M. Assembly of Graphene Oxide at the Crude Oil/Water Interface: A New Approach to Efficient Demulsification. *Energy Fuels* **2016**, *30*, 3355–3364.
- (18) McCoy, T. M.; Pottage, M. J.; Tabor, R. F. Graphene Oxide-Stabilized Oil-in-Water Emulsions: PH-Controlled Dispersion and Flocculation. *J. Phys. Chem. C* **2014**, *118*, 4529–4535.
- (19) Kalashnikova, I.; Bizot, H.; Cathala, B.; Capron, I. Modulation of Cellulose Nanocrystals Amphiphilic Properties to Stabilize Oil/Water Interface. *Biomacromolecules* **2012**, *13*, 267–275.
- (20) Xia, Z.; Lin, C. G.; Yang, Y.; Wang, Y.; Wu, Z.; Song, Y. F.; Russell, T. P.; Shi, S. Polyoxometalate-Surfactant Assemblies: Responsiveness to Orthogonal Stimuli. *Angew. Chem., Int. Ed.* **2022**, *61*, No. e202203741.
- (21) Feng, T.; Hoagland, D. A.; Russell, T. P. Assembly of Acid-Functionalized Single-Walled Carbon Nanotubes at Oil/Water Interfaces. *Langmuir* **2014**, *30*, 1072–1079.
- (22) ShamsiJazeyi, H.; Hirasaki, G. J.; Verduzco, R. Sacrificial Agent for Reducing Adsorption of Anionic Surfactants. *Proc. SPE Int. Symp. Oilfield Chem.* **2013**, *1*, 214–229.

- (23) de Avila, J. N. L.; de Araujo, L. L. G. C.; Drexler, S.; de Almeida Rodrigues, J.; Nascimento, R. S. V. Polystyrene Nanoparticles as Surfactant Carriers for Enhanced Oil Recovery. *J. Appl. Polym. Sci.* **2016**, *133*, 43789.
- (24) Zhou, Y.; Wu, X.; Zhong, X.; Sun, W.; Pu, H.; Zhao, J. X. Surfactant-Augmented Functional Silica Nanoparticle Based Nanofluid for Enhanced Oil Recovery at High Temperature and Salinity. ACS Appl. Mater. Interfaces 2019, 11, 45763–45775.
- (25) Nourafkan, E.; Hu, Z.; Wen, D. Nanoparticle-Enabled Delivery of Surfactants in Porous Media. *J. Colloid Interface Sci.* **2018**, *519*, 44–57.
- (26) Hirasaki, G. J.; Miller, C. A.; Puerto, M. Recent Advances in Surfactant EOR. *Proc. SPE Annu. Tech. Conf. Exhib.* **2008**, *2*, 1108–1142.
- (27) Zhang, J.; Lin, Y.; Lin, Z.; Wei, Q.; Qian, J.; Ruan, R.; Jiang, X.; Hou, L.; Song, J.; Ding, J.; Yang, H. Stimuli-Responsive Nanoparticles for Controlled Drug Delivery in Synergistic Cancer Immunotherapy. *Adv. Sci.* **2022**, *9*, No. 2103444.
- (28) Mitchell, M. J.; Billingsley, M. M.; Haley, R. M.; Wechsler, M. E.; Peppas, N. A.; Langer, R. Engineering Precision Nanoparticles for Drug Delivery. *Nat. Rev. Drug Discovery* **2021**, *20*, 101–124.
- (29) Galán-Jiménez, M. d. C.; Mishael, Y. G.; Nir, S.; Morillo, E.; Undabeytia, T. Factors Affecting the Design of Slow Release Formulations of Herbicides Based on Clay-Surfactant Systems. A Methodological Approach. *PLoS One* **2013**, *8*, No. e59060.
- (30) Alsmaeil, A. W.; Enotiadis, A.; Hammami, M. A.; Giannelis, E. P. Slow Release of Surfactant Using Silica Nanosized Capsules. *SPE J.* **2020**, 25, 3472–3480.
- (31) Alsmaeil, A. W.; Hammami, M. A.; Enotiadis, A.; Kanj, M. Y.; Giannelis, E. P. Encapsulation of an Anionic Surfactant into Hollow Spherical Nanosized Capsules: Size Control, Slow Release, and Potential Use for Enhanced Oil Recovery Applications and Environmental Remediation. ACS Omega 2021, 6, 5689–5697.
- (32) Costa, L.; Li-Destri, G.; Pontoni, D.; Konovalov, O.; Thomson, N. H. Liquid-Liquid Interfacial Imaging Using Atomic Force Microscopy. *Adv. Mater. Interfaces* **2017**, *4*, No. 1700203.
- (33) Costa, L.; Li-Destri, G.; Thomson, N. H.; Konovalov, O.; Pontoni, D. Real Space Imaging of Nanoparticle Assembly at Liquid-Liquid Interfaces with Nanoscale Resolution. *Nano Lett.* **2016**, *16*, 5463–5468.
- (34) Chai, Y.; Hasnain, J.; Bahl, K.; Wong, M.; Li, D.; Geissler, P.; Kim, P. Y.; Jiang, Y.; Gu, P.; Li, S.; Lei, D.; Helms, B. A.; Russell, T. P.; Ashby, P. D. Direct Observation of Nanoparticle-Surfactant Assembly and Jamming at the Water-Oil Interface. *Sci. Adv.* **2020**, *6*, No. eabb8675.
- (35) Chai, Y.; Lukito, A.; Jiang, Y.; Ashby, P. D.; Russell, T. P. Fine-Tuning Nanoparticle Packing at Water-Oil Interfaces Using Ionic Strength. *Nano Lett.* **2017**, *17*, 6453–6457.
- (36) Toor, A.; Forth, J.; Bochner De Araujo, S.; Merola, M. C.; Jiang, Y.; Liu, X.; Chai, Y.; Hou, H.; Ashby, P. D.; Fuller, G. G.; Russell, T. P. Mechanical Properties of Solidifying Assemblies of Nanoparticle Surfactants at the Oil-Water Interface. *Langmuir* **2019**, 35, 13340–13350.
- (37) Zhang, Z.; Jiang, Y.; Huang, C.; Chai, Y.; Goldfine, E.; Liu, F.; Feng, W.; Forth, J.; Williams, T. E.; Ashby, P. D.; Russell, T. P.; Helms, B. A. Guiding Kinetic Trajectories between Jammed and Unjammed States in 2D Colloidal Nanocrystal-Polymer Assemblies with Zwitterionic Ligands. *Sci. Adv.* **2018**, *4*, No. eaap8045.
- (38) Keane, R. K.; Hong, W.; He, W.; Teale, S.; Bancroft, R.; Dinsmore, A. D. Adsorption of Hydrophilic Silica Nanoparticles at Oil-Water Interfaces with Reversible Emulsion Stabilization by Ion Partitioning. *Langmuir* **2022**, *38*, 2821–2831.
- (39) Whitby, C. P.; Fornasiero, D.; Ralston, J. Effect of Oil Soluble Surfactant in Emulsions Stabilised by Clay Particles. *J. Colloid Interface Sci.* **2008**, 323, 410–419.
- (40) Afekare, D.; Garno, J. C.; Rao, D. Insights into Nanoscale Wettability Effects of Low Salinity and Nanofluid Enhanced Oil Recovery Techniques. *Energies* **2020**, *13*, 4443.

- (41) Shi, C.; Xie, L.; Zhang, L.; Lu, X.; Zeng, H. Probing the Interaction Mechanism between Oil Droplets with Asphaltenes and Solid Surfaces Using AFM. *J. Colloid Interface Sci.* **2020**, 558, 173–181.
- (42) Brzozowska, A. M.; Duits, M. H. G.; Mugele, F. Stability of Stearic Acid Monolayers on Artificial Sea Water. *Colloids Surf., A* **2012**, 407, 38–48.
- (43) Phan, M. D.; Lee, J.; Shin, K. Collapsed States of Langmuir Monolayers. J. Oleo Sci. 2016, 65, 385–397.
- (44) Moore, F. G.; Richmond, G. L. Integration or Segregation: How Do Molecules Behave at Oil/Water Interfaces? *Acc. Chem. Res.* **2008**, *41*, 739–748.
- (45) Farinmade, A.; Ojo, O. F.; Trout, J.; He, J.; John, V.; Blake, D. A.; Lvov, Y. M.; Zhang, D.; Nguyen, D.; Bose, A. Targeted and Stimulus-Responsive Delivery of Surfactant to the Oil-Water Interface for Applications in Oil Spill Remediation. ACS Appl. Mater. Interfaces 2020, 12, 1840–1849.
- (46) Smits, J.; Giri, R. P.; Shen, C.; Mendonça, D.; Murphy, B.; Huber, P.; Rezwan, K.; Maas, M. Synergistic and Competitive Adsorption of Hydrophilic Nanoparticles and Oil-Soluble Surfactants at the Oil-Water Interface. *Langmuir* **2021**, *37*, 5659–5672.
- (47) Hosseinpour, S.; Götz, V.; Peukert, W. Effect of Surfactants on the Molecular Structure of the Buried Oil/Water Interface. *Angew. Chem., Int. Ed.* **2021**, *60*, 25143–25150.
- (48) Hua, X.; Bevan, M. A.; Frechette, J. Competitive Adsorption between Nanoparticles and Surface Active Ions for the Oil-Water Interface. *Langmuir* **2018**, 34, 4830–4842.
- (49) Acedo-Carrillo, J. I.; Rosas-Durazo, A.; Herrera-Urbina, R.; Rinaudo, M.; Goycoolea, F. M.; Valdez, M. A. Zeta Potential and Drop Growth of Oil in Water Emulsions Stabilized with Mesquite Gum. *Carbohydr. Polym.* **2006**, *65*, 327–336.
- (50) Gan, W.; Wu, W.; Yang, F.; Hu, D.; Fang, H.; Lan, Z.; Yuan, Q. The Behavior of Hydroxide and Hydronium Ions at the Hexadecane—Water Interface Studied with Second Harmonic Generation and Zeta Potential Measurements. *Soft Matter* **2017**, *13*, 7962–7968.
- (51) Jayme, M. L.; Dunstan, D. E.; Gee, M. L. Zeta Potentials of Gum Arabic Stabilised Oil in Water Emulsions. *Food Hydrocolloids* **1999**, *13*, 459–465.
- (52) Lee, Y. L.; Yang, Y. C.; Shen, Y. J. Monolayer Characteristics of Mixed Octadecylamine and Stearic Acid at the Air/Water Interface. *J. Phys. Chem. B* **2005**, *109*, 4662–4667.